JOURNAL OF CATALYSIS **170,** 377–389 (1997)
ARTICLE NO. CA971747

Kinetics of Rapid Heterogeneous Reactions on the Nanometer Scale

V. P. Zhdanov*,† and B. Kasemo*

*Department of Applied Physics, Chalmers University of Technology, S-412 96 Göteborg, Sweden; and †Boreskov Institute of Catalysis, Russian Academy of Sciences, Novosibirsk 630090, Russia

Received December 26, 1996; revised April 28, 1997; accepted May 5, 1997

Steady-state kinetics of catalytic reactions, occurring on supported catalyst particles of the nanometer size, are analyzed by employing two schemes taking into account respectively (i) the interplay of reactions on different facets of the catalyst particle and (ii) the possibility of adsorption of reactants on the support followed by diffusion to the catalyst. A chosen model reaction, $2A + B_2 \rightarrow 2AB$, is assumed to involve monomolecular A adsorption, dissociative B_2 adsorption, and the Langmuir–Hinshelwood step resulting in the formation of AB. This reaction mimics such practically important catalytic processes as CO oxidation on Pt, Rh, or Pd, and its kinetics for the infinite surface have been explored in detail during the past decade. The results obtained in the present study demonstrate that the kinetics on the nanometer-size catalyst particles can be remarkably different from those corresponding to the infinite surface. This conclusion is drawn on the basis of Monte Carlo simulations with realistic ratio between the rates of reaction and reactant diffusion [scheme (i)] and self-consistent equations explicitly describing A diffusion on the support and the reaction steps on the catalyst [scheme (ii)].

1. INTRODUCTION

Kinetics simulations in heterogeneous catalysis are of central importance, both fundamentally, in order to understand the intimate details of the reaction behavior, and practically, to model reactor performance. In such simulations, the rate constants and the overall kinetics (elementary steps, coverage dependence, etc.) are usually obtained either from single crystal studies in ultrahigh vacuum or empirically from real catalysts. The latter frequently consist of active nanometer-sized catalyst particles on more or less inactive supports. Potential differences between the "ideal" single crystal catalysts of essentially infinite lateral extension and the 10- to 100-nm-sized catalyst particles on a support, have long been realized and expressed as the "structure gap." Solid understanding of the special kinetic effects, which are possible with decreasing the size of catalyst particles down to a few nanometers, is, however, lacking. It is therefore important to develop simulation schemes in which reactions occur on finite supported particles. The importance of such simulations is expected to increase both because of the practical relevance and because modern nanofabrication technologies (1) provide the opportunity to create mesoscopic model systems of supported catalysts, with a controlled size, shape, and distribution on the support. For example, electron beam lithography makes it possible (2) to prepare model catalysts consisting of platinum particles of 20–50 nm diameter and 15–20 nm height at 30–200 nm spacing on an oxidized silicon wafer.

With respect to the kinetics, the structure gap problem can be divided into three main categories:

(i) The first one concerns reactions on nanometer-sized catalyst particles (here assumed to be monocrystalline), exposing different crystal faces. Since it is well known from single crystal studies that the kinetics may be very different on different crystal faces, in general one cannot expect that the kinetics on nanometer particles can be directly represented by the kinetics of a single *(klm)* surface. As shown in this paper, it cannot even be represented by a superposition of the kinetics from different crystal faces exposed by the nanometer-sized catalysts. The reason is that adjacent crystal faces communicate with each other by surface diffusion, which constitutes a unique kinetic feature of the nanometer particles.

(ii) The second category of kinetic effects associated uniquely with small catalyst particles on a support is the spillover effect, consisting generally of adsorption on the support followed by diffusion from the support to the catalyst particle or vice versa. Normally the support is assumed to be catalytically inactive, but not always. A prominent example is the so-called oxygen storage in car exhaust catalysts (3) where a metal oxide constitutes an oxygen uptake/release function for reactions occurring on the noble metal catalyst.

(iii) The third category is connected with chemical modification of the highly dispersed catalyst particles by the support.

In the present paper, we analyze the first two factors mentioned above, namely (i) the interplay of the reactions on different facets of a catalyst particle and (ii) the possibility of adsorption of reactants on the support followed by

0021-9517/97 $25.00

diffusion to the catalyst (Sections 2 and 3, respectively). Both factors are expected to be especially important for rapid *bistable* reactions, because in this case the reaction regimes on different facets of a catalyst may be particularly different and the adsorption overlayer is often far from adsorption–desorption equilibrium. The most interesting feature of rapid reactions is *kinetic* phase transitions (for the review, see Ref. (4)), and we will pay special attention to such transitions.

An analysis of rapid reactions at the nanometer-length scale almost inevitably requires the use of MC simulations. Such simulations are far from straightforward if one wants to understand situations corresponding to real reactions, because in this case the ratio of the rate constants of different steps varies over many orders of magnitude. The weakness of the available MC simulations of rapid reactions is that, due to computational limitations, they as a rule use unrealistically low surface mobilities. This point, already noted in the reviews (4, 5), is discussed in detail in our paper (Section 2). We show that the problems in this field might in principle be solved by employing MC algorithms specially designed to treat the limit when the ratio of the rate constants of different steps is high. Such algorithms are expected to be widely used in further simulations.

A brief preliminary report about the results presented in this paper was recently published elsewhere (6). The present paper is a considerable extension and contains several new results and a detailed discussion.

2. INTERPLAY OF REACTIONS ON DIFFERENT FACETS

General Comments

Measurements of the partial reaction rates corresponding to different facets of nm-size catalyst particle are hardly possible. For this reason, experimental data in this area are very limited. As one of few examples, we mention an interesting study by Gorodetskii *et al.* (7) of the kinetics of the hydrogen–oxygen reaction on Pt at low pressures ($\sim 10^{-6}$ bar) and room temperature. On a macroscopic Pt(100) single crystal the reaction was found to reach a steady state with a uniform distribution of adsorbates. But on the Pt tip of a field ion microscope, on which several different crystal planes are exposed, the reaction rate displayed sustained temporary oscillations [on a (100) facet of 40 nm diameter]. This effect was associated with continuously changing distributions of the adsorbed species in the form of propagating waves, which were generated by coupling of reactions occurring on adjacent crystal planes.

Simulations of rapid catalytic reactions, with special focus on the interplay between reactions on different facets of the catalyst particle, are to our knowledge lacking. There are however a few studies of the reaction kinetics on catalytic "patches" (8–12) with reactant diffusion ("spillover" (21)) between patches. The results obtained in the latter studies are relevant for our discussion because different facets of a catalyst particle can sometimes be formally treated as a set of patches. For this reason, it is of interest to review Refs. (8–12) in some detail. First, however, we need to recall the relationship between the reaction and diffusion rates in rapid reactions.

Reaction Rates vs Diffusion Rates

The type of approximations which should be used in simulations depends on the ratio between the rate constants of different steps. As an example, we consider below the $2A + B_2 \rightarrow 2AB$ reaction occurring via the standard Langmuir–Hinshelwood (LH) mechanism,

$$A_{\text{gas}} \rightleftharpoons A_{\text{ads}}, \qquad [1]$$

$$(B_2)_{\text{gas}} \rightarrow 2B_{\text{ads}}, \qquad [2]$$

$$A_{\text{ads}} + B_{\text{ads}} \rightarrow (AB)_{\text{gas}}. \qquad [3]$$

This scheme mimics, e.g., CO or hydrogen oxidation on the noble metal catalysts Pt, Pd, and Rh (A then stands for CO or hydrogen, and B_2 for O_2). Hydrogen adsorption is of course dissociative, and H_2O formation occurs in a few steps, but the general features of the kinetics of hydrogen oxidation are the same as for CO oxidation (at least on Pt (4)).

To compare the rates of reaction and diffusion, it is useful to employ the Arrhenius form (with $k_B = 1$) to represent the rate constants for diffusion jumps of A and B particles to nearest-neighbor vacant sites and for the reaction between two nearest-neighbor reactants, respectively,

$$k_{\text{dif}}^A = \nu_{\text{dif}}^A \exp\left(-E_{\text{dif}}^A/T\right), \qquad [4]$$

$$k_{\text{dif}}^B = \nu_{\text{dif}}^B \exp\left(-E_{\text{dif}}^B/T\right), \qquad [5]$$

$$k_{\text{r}} = \nu_{\text{r}} \exp(-E_{\text{r}}/T). \qquad [6]$$

The ratio of these rate constants depend first of all on the values of the activation energies, because the preexponential factors for surface diffusion are close to those for the LH step (at least according to the transition state theory (33)).

In the case of CO oxidation on Pt(111), we have $E_{\text{dif}}^A \simeq$ 4–7 kcal/mol (13) and $E_{\text{r}} \simeq 24$ kcal/mol (14). Accurate measurements of the activation energy for oxygen diffusion on Pt(111) are lacking. The field-emitter measurements (see the review (13)) indicate that $E_{\text{dif}}^B \simeq 27$ kcal/mol at relatively high coverages. The interpretation of these results is, however, not simple (due to the boundary effects). The recent STM measurements (15) carried out in a relatively small temperature range (190–204 K) show that $E_{\text{dif}}^B \simeq 9.9$ kcal/mol and $D_0 \simeq 10^{-6.3}$ cm^2/s (the latter value is low compared to the "normal" one, $D_0 = 10^{-3}$ cm^2/s). Some

indirect data concerning oxygen diffusion can be obtained from recent studies of CO oxidation on Pt(111) (Ref. (16, Fig. 3)), which indicate that two *differently* prepared overlayers with *equal initial coverages* display different kinetic behavior at 350 K. Taking into account that CO diffusion is fairly rapid, we can conclude from this observation that oxygen was not able to reach equilibrium at 350 K during the period $\tau \approx 10$ s (τ is the time scale of the measurements (16)). Mathematically, this means that

$$\tau \nu_{\rm dif}^{B} \exp\left(-E_{B}^{\rm dif}/T\right) < 1. \qquad [7]$$

Assuming a normal pre-exponential factor, $\nu_{\rm dif}^{B} = 10^{13}$ s^{-1}, we obtain from the equation above that $E_{\rm dif}^{B} > 22$ kcal/mol. Combining this value with that quoted in Ref. (13), we get $E_{\rm dif}^{B} \approx 25$ kcal/mol as a probable value. In this case, we have for CO oxidation on Pt(111)

$$k_{\rm dif}^{B} \approx k_{\rm r} \ll k_{\rm dif}^{A}. \qquad [8]$$

If, however, the activation energy for oxygen diffusion is low, $\simeq$9.9 kcal/mol (15), we obtain

$$k_{\rm r} \ll k_{\rm dif}^{B} \ll k_{\rm dif}^{A}. \qquad [9]$$

The latter condition corresponds to the mean-field (MF) approximation.

For hydrogen oxidation on Pt(111), the activation energies for the reaction steps are not well established. Analyzing the literature (see, e.g., the discussion in Ref. (17)), one can conclude that the activation barriers for the LH steps are expected to be about 5–7 kcal/mol and for hydrogen diffusion even lower. Accordingly, we have

$$k_{\rm dif}^{B} \ll k_{\rm r} \ll k_{\rm dif}^{A}. \qquad [10]$$

There were, however, reports (18) that the reaction might be limited by oxygen diffusion to active centers. At present, it is not clear whether this conclusion is correct, because the reaction was studied at relatively low temperatures where the oxygen overlayer might be far from equilibrium due to limited oxygen mobility (as it follows from the results reported in Ref. (16)). If the reaction is really controlled by oxygen diffusion to active centers, condition [10] of course does not hold.

Employing the activation energies for elementary steps for CO or hydrogen oxidation on Pt(111), one can easily estimate the average diffusion length per unit time and the diffusion length prior to reaction, respectively, as shown in Fig. 1.

In summary, we may conclude that A diffusion is usually *rapid* compared to the LH step, while the rate constant for the LH step might be higher than (Eq. [10]), close to (Eq. [8]), or lower than (Eq. [9]) that for B diffusion. Physically, this means that the distribution of A particles on the surface (at least on flat facets) should be close to equilibrium. On the other hand, the distribution of B particles might be far from equilibrium.

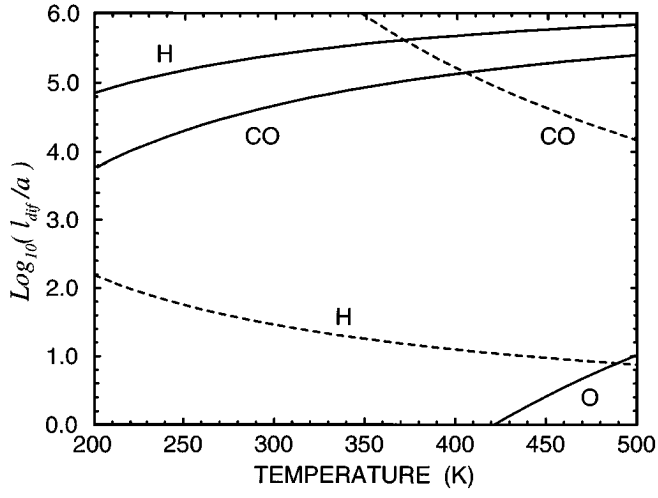

FIG. 1. Typical diffusion lengths, $l_{\rm dif}$, for H, CO, and O on Pt(111) as a function of temperature. Solid lines show the average diffusion length, $l_{\rm dif}/a = [\tau \nu_{\rm dif} \exp(-E_{\rm dif}/T)]^{1/2}$ (a is the lattice spacing), for $\tau = 1$ s with $\nu_{\rm dif} = 10^{13}$ s^{-1} and $E_{\rm dif} = 3$ (H), 5 (CO), and 25 (O) kcal/mol. Dashed lines represent the average diffusion length of H and CO during their lifetime in the course of reaction, $l_D/a \approx \exp[(E_{\rm r} - E_A^{\rm dif})/2T]$, for $E_{\rm r} - E_A^{\rm dif} = 4$ (H) and 19 (CO) kcal/mol.

Previous Simulations

Brosilow *et al.* (8) have simulated low-temperature ($\sim$200 K) CO oxidation on Pt islands deposited on oxide support. Their model consisted of an $L \times L$ square lattice (L is the lattice size) containing a circle of radius $R < L/2$ ($R \simeq 10$–100). All the sites inside and on the circle were assumed to correspond to Pt and the sites with $R > L/2$ were oxide sites. The reaction was allowed to occur on Pt sites and also on Pt/oxide boundary sites via the standard LH mechanism (Eqs. [1]–[3]) with irreversible A and B_2 adsorption. *Adsorbate diffusion was neglected.* Reaction between nearest-neighbor reactants was assumed to be *instantaneous*. For boundary sites, the simulation algorithm was chosen so that whenever a B atom on a site outside the circle of radius R reacted with A from inside the circle, the resulting unoccupied site outside the circle was immediately refilled by B. The arriving molecules were selected to be A with a probability p and B_2 with the probability $1 - p$ ($p \le 1$ is the dimensionless A pressure). In the limit $R \to \infty$, this model predicts (see Ref. (19), the review (4), or Fig. 3) a reactive steady state in a very narrow reaction window, $p_1 < p < p_2$, with $p_1 = 0.389 \pm 0.005$ and $p_2 = 0.525 \pm 0.001$. The surface is completely "poisoned" by B particles for $p < p_1$ and by A particles for $p > p_2$. With a finite radius of the Pt island, the reaction rate at $p < p_2$ was in fact found to be the same as for the infinite surface (the surface is

poisoned by B at $p < p_1$). For $p > p_2$, the reaction running on the patch was shown to have a finite rate, in contrast to the infinite surface, due to reaction of A molecules arriving on the boundary sites. The reaction rate predicted for $p > p_2$, is however, fairly low.

The results obtained in Ref. (8) are interesting from a tutorial point of view, but unrealistic because CO diffusion on Pt is rather rapid even at $T = 200$ K (Fig. 1). Taking into account the latter point, Savchenko and Efremova (9) have tried, by employing the algorithm from Ref. (20), to simulate CO oxidation (steps [1]–[3]) with rapid CO diffusion occurring via jumps to nearest-neighbor vacant sites on a 100×100 lattice containing two types of rectangular strips with a width of $10a$ (a is the lattice spacing). The number of jumps used for CO diffusion was up to 100. Oxygen diffusion was neglected. The reaction between nearest-neighbor reactants was considered to be *instantaneous* (as in Ref. (8)). The latter (in combination with rapid CO diffusion via nearest-neighbor sites) corresponds mathematically to

$$k_{\mathrm{dif}}^{B} \ll k_{\mathrm{dif}}^{A} \ll k_{\mathrm{r}}. \qquad [11]$$

This condition is different from conditions [8], [9], and [10].

To emphasize the difference, it is instructive to discuss briefly the reaction kinetics corresponding to conditions [10] and [11] in the situation when the surface is primarily covered by B particles (oxygen) as shown, for example, in Fig. 2. When the reaction is rapid compared to adsorption, the arriving A molecules will rapidly react with B particles for both cases [10] and [11]. The relative reaction probabilities of B particles in different sites will, however, be different for conditions [10] and [11], respectively. If A diffusion is rapid compared to reaction (Eq. [10]), every A particle will on the average perform a large number of diffusion jumps to vacant sites (including those having B neighbors) before reaction. This means that the A particles will be distributed on the surface *at random*. In this case, the reaction probabilities for B particles marked, e.g., by numbers 1 and 2 will be equal because both particles have four vacant nearest-neighbor sites which can potentially be occupied by A particles with the same probability.

If the reaction is instead rapid compared to A diffusion (Eq. [11]), an A particle will react with the *first* nearest-neighbor B particle on its way. In the latter case, the reaction probability for the B particle located in site 1 will be much lower than that for the B particle located in site 2, simply because the probability of A adsorption near the former B particle, surrounded by other B particles (in next-nearest-neighbor sites) is much lower than that for the latter B particle, which has plenty of adjacent vacant sites for A adsorption. Thus, the reaction kinetics corresponding respectively to conditions [10] and [11] are expected to be *quantitatively* different.

Savchenko *et al.* (10–12) have also employed the MF approximation to analyze the kinetics of a few model reactions on the surface consisting of two types of patches. Diffusion between patches has not been treated explicitly. Instead, the patches were described in analogy with two well-stirred reactors. In particular, the A reactant flux from patch 1 to patch 2 was considered to be proportional to the product of the average A coverage of the former patch and the fraction of vacant sites on the latter patch (this approximation was earlier used by Silveston *et al.* (22, 23) (see Section 3)). For the simplest $A \rightarrow B$ reaction (10) and for the scheme mimicking CO oxidation (11), it was shown (in analogy with MC simulations (9)) that the reaction rate on the spotted surface might be higher than on the uniform surface. For the latter scheme, it was also demonstrated (12) that the interplay between patches may change the number of steady states.

The merit of the MF approximation is its simplicity. The disadvantage is that the diffusion of both reactants is implicitly assumed to be rapid, i.e.,

$$\min\left(k_{\mathrm{dif}}^{B}, k_{\mathrm{dif}}^{A}\right) \gg k_{\mathrm{r}}. \qquad [12]$$

The latter condition is not always fulfilled for rapid reactions.

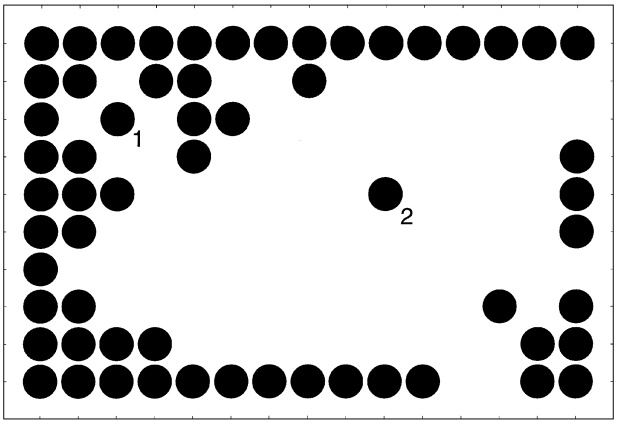

FIG. 2. Arrangement of B particles (filled circles) on a square lattice.

Algorithm and Results of Simulations

Compared to earlier works, we want to explore the kinetics of the $2A + B_2 \rightarrow 2AB$ reaction (steps [1]–[3]) with irreversible A adsorption in the nanometer-size limit and with a realistic ratio between the rate constants of different steps. In particular, we are interested in the case when A diffusion is rapid compared to the reaction which in turn is rapid compared to B diffusion (Eq. [10]). The idea making it possible to realize such calculations is fairly simple (24, 25): if diffusion of A particles is rapid, one may distribute these reactants on the available sites (which are free of B particles) either at random, if there is no lateral adsorbate-adsorbate

interactions, or according to the canonical distribution when there are finite lateral interactions. This natural prescription, assuming a canonical distribution of A particles on all the non-B sites, even if different subsets of these sites are topologically disconnected by B-regions, is completely correct for the "precursor" mechanism of A diffusion. If, however, the diffusion occurs only via nearest-neighbor jumps, the rule outlined above is just a reasonable approximation (25). To simulate rapid diffusion of A particles, we use the prescription proposed in Refs. (24) and (25). In addition, our MC algorithm outlined below takes *explicitly* into account that the LH step is rapid compared to adsorption (the algorithms described earlier (24, 25) are not specially designed for the case under consideration and are for this reason too time consuming).

If A diffusion is rapid compared to the LH step and in turn this step is rapid compared to adsorption, one of the reactant coverages will at steady-state state always be low compared to the other. Taking into account that the rates of A and B diffusion are essentially different (A diffusion is fast, and B diffusion is negligible), we can use different techniques to analyze the situations when the dominant adsorbate is A or B, respectively. If the surface is predominantly covered by A particles, we can employ the MF approximation to describe the reaction because A particles are distributed at random (we ignore lateral interactions). This case, however, is not interesting (for the infinite overlayer, the surface will, for example, be completely covered by A particles). For this reason, we focus our attention on the situation when the surface is predominantly covered by B particles. If the reaction rate constant for the LH step is very high, the average number of A particles on a lattice with a limited number of sites (e.g., 100×100) will be much lower than unity. Physically, this means that in this limit every A particle arriving at the surface will react with very high probability *before* the next A particle arrives. Thus, we only need to keep B particles on the $L \times L$ lattice. Then, the MC algorithm is as follows: (1) The arriving molecule is chosen to be A with a probability p and B_2 with the probability $1-p$ ($p \leq 1$ is the dimensionless A impingement rate). (2) If the arriving molecule is A, a site (site 1) on the lattice is chosen at random. If that site is occupied, the trial ends. Otherwise, A reacts. In particular, an adjacent site (site 2) is randomly chosen, and if this site is occupied by a B particle this particle is removed from the lattice (i.e., AB leaves the surface). If the adjacent site is vacant, the A particle is moved from site 1 to another vacant site, randomly chosen on the lattice, and then it again tries to react as described above. The latter two steps (movement to a new site and an attempt to react) are repeated until a successful reaction event occurs. (3) If the arriving molecule is B_2, two adjacent sites are chosen at random. If either site is occupied, the trial ends. Otherwise, B_2 dissociates and adsorbs on the chosen sites.

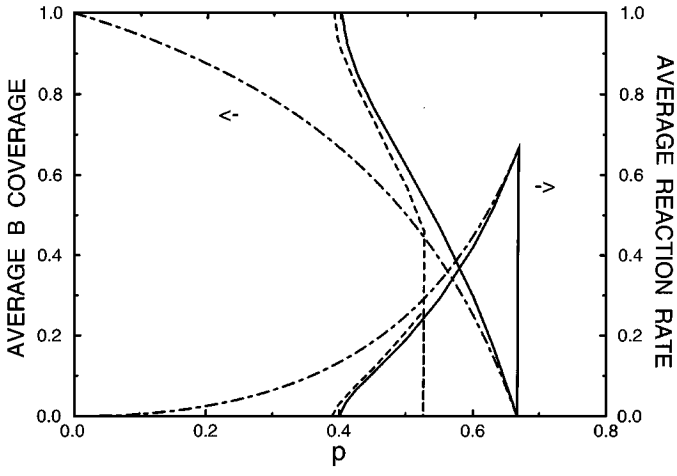

FIG. 3. Reaction rate and B coverage for rapid $2A + B_2 \rightarrow 2AB$ reaction with irreversible adsorption of reactants (the adsorbed overlayer is infinite). Dot-dashed lines show the MF results (4) (in this case, the system only exhibits the first-order kinetic phase transition with the spinodal point $p_2 = 2/3$; the position of the equistability line (not shown), dependent on the ratio between the reactant diffusion coefficients, can be calculated analytically (e.g., $p^* = 0.594$ for $D_A = D_B$)). Thin dashed lines correspond to immobile reactants (19) (the continuous and first-order transitions occur at $p_1 = 0.389 \pm 0.005$ and $p_2 = 0.525 \pm 0.001$, respectively; the position of the equistability line in fact coincides with the spinodal point; inside the reaction window, the surface contains A and B particles, but the A coverage (not shown) is very low). Solid lines (our results for a 500×500 lattice and 10^4 MCS) are for rapidly diffusing A particles and immobile B particles (in this case, the continuous and first-order transitions occur at $p_1 = 0.401 \pm 0.005$ and $p_2 = 2/3$, respectively; the equistability line (not shown) is located at $p^* = 4/7 = 0.571$ (the analytical result (4))).

Complementing rules 1–3 by periodic boundary condition, we have first simulated the reaction kinetics for the infinite adsorbed overlayer. In this case, the model exhibits kinetic phase transitions (Fig. 3). Corresponding critical values of p can accurately be calculated only if the lattice size is relatively large. We used a 500×500 lattice with 10^4 MC steps (1 MCS corresponds by definition to $L \times L$ attempts of adsorption). According to our analysis, the surface is "poisoned" by B particles for $p < p_1 = 0.401 \pm 0.005$ and by A particles for $p > p_2 = 0.667 \pm 0.003$. The former critical value is close to that predicted (19) for immobile A adsorption ($p_1 = 0.389 \pm 0.005$), and the latter one coincides with the MF result (4) ($p_2 = 2/3$). Typical arrangements of B particles on the lattice for p inside the reaction window are shown in Fig. 4.

We now turn to the nanometer-size regime. To demonstrate the magnitude by which the kinetics occurring on the nanometer-size crystals differ from those calculated for the infinite adsorbed overlayer, we approximate one facet of a catalyst particle by a 50×50 lattice corresponding to $\sim$10 nm dimension. An interplay between the reaction on this facet and neighboring facets is imitated by introducing special boundary conditions: the bottom and top rows of sites are assumed to be adjacent to A-poisoned

facets, and the left- and right-hand-side rows are adjacent to *B*-poisoned facets. (In a real system, this situation would be realized if, e.g., the adsorption probability ratio for *A* versus *B* particles were larger and smaller, respectively, on the top/bottom and left/right adjacent facets compared to the middle facet.) In particular, *B* particles deposited by adsorption on the bottom or top rows are assumed to react instantaneously with *A* particles sitting on the sites belonging to adjacent facets. Accordingly, an *A* particle "jumping" after adsorption in order to find a partner may react not only with *B* particles located on the facet where it was adsorbed but also with *B* particles on adjacent facets, provided that it reaches the left- and right-hand-side rows of sites (the game rules are the same as described above). Refilling of *A* and *B* particles on the boundary sites of adjacent facets is considered to be rapid (this assumption is reasonable because the adjacent sites are poisoned by *A* or *B* particles).

With the boundary conditions introduced, the central facet is almost completely poisoned by *B* for $p < p_1$ ($p_1 = 0.401$ and $p_2 = 2/3$ are the critical parameters for the infinite overlayer). Reaction events occur in this case (with low local rate (Fig. 5)) only near the bottom and top rows of sites (Fig. 6a) at the interface between the *A* and *B* covered facets. At $p_1 < p < p_2$, the reaction behavior on the central facet is close to that predicted for the infinite overlayer (see Figs. 5 and 7, and cf. Figs. 4 and 6b). The dramatic difference in the kinetics is observed at $p > p_2$. Here, the infinite surface is completely poisoned by *A*, i.e., the overlayer is in the unreactive state (a similar situation occurs if the reaction of *immobile* reactants takes place on a circular spot with the "hard" *B* boundary condition (8)). In contrast, the central facet is almost empty (Fig. 6c) and the reaction rate is high, because the large relative impingement rate of *A* particles, causing poisoning of the infinite surface, is compensated on the facet by reaction of some of these *A* particles at the left- or right-hand-side boundary sites, filled by *B* particles. This compensation will be maintained until a kinetic phase transition to an *A* covered surface takes place on the left- and right-hand-side adjacent facets. The exact *p*-value where this occurs is determined by the ration of the sticking coefficients for *A* and B_2, respectively, on the left- and right-hand-side adjacent facets. In the present case, this ratio is assumed to be low and the kinetic phase transition occurs only when $p \to 1$.

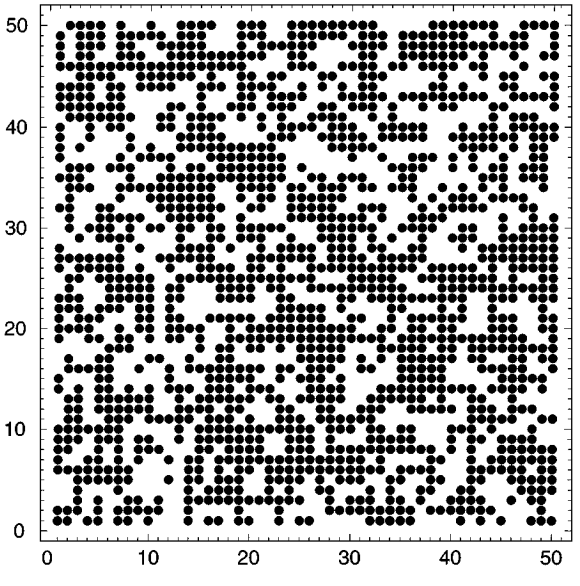

FIG. 4. A 50×50 fragment of the 500×500 lattice after 10^4 MCS at $p = 0.5$. Filled circles show *B* particles.

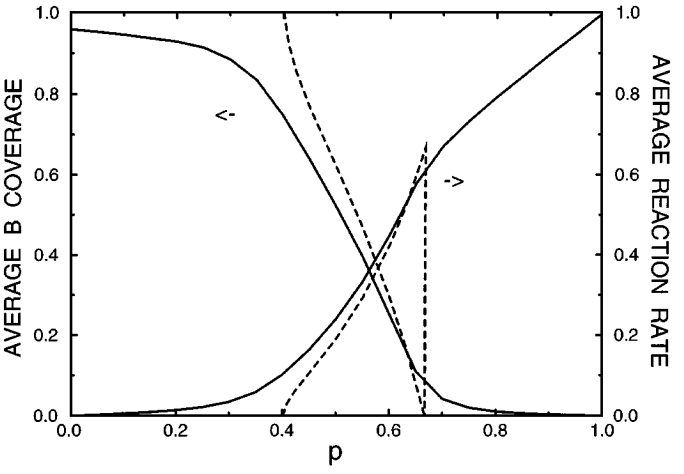

FIG. 5. Average reaction rate (*A* molec. site^{-1} MCS^{-1}) and *B* coverage after 10^4 MCS. Solid and dashed lines corresponds to a 50×50 lattice (with the boundary conditions described in the text) and to the infinite adsorbed overlayer, respectively.

In summary, our MC simulations carried out for the $2A + B_2 \to 2AB$ reaction, with a realistic ratio between the rates of the elementary steps, show that the interplay between the reaction kinetics on different facets of nanometer-sized active catalyst particles might increase the reaction rate compared to the infinite crystal. This effect is qualitatively the same, but quantitatively even larger, compared to that predicted earlier for reactions occurring on patches (8–12). Some practical implications of this are discussed in Section 4.

3. REACTANT SUPPLY VIA THE SUPPORT (SPILLOVER)

Previous Simulations

A factor of both fundamental and practical importance in catalysis, which might change the reaction kinetics on supported systems, is the possibility of adsorption of reactants on the support followed by diffusion to the catalyst and vice versa (Fig. 8). The role of this so-called spillover channel has already been discussed in the literature. In particular, there are experimental reports that the supply of

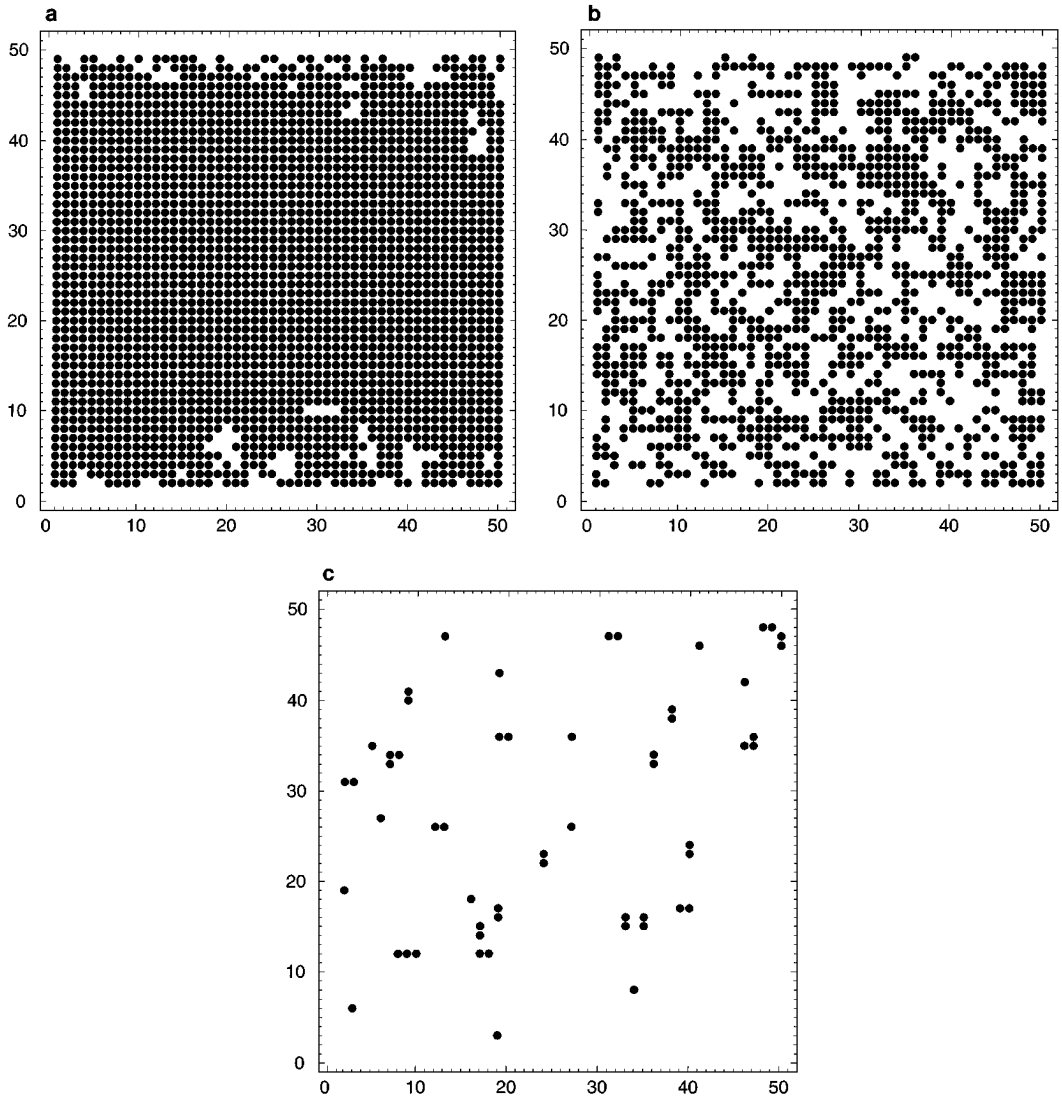

FIG. 6. Arrangement of B particles on a 50×50 lattice (with the boundary conditions described in the text) after 10^4 MCS for $p = 0.25$ (a), 0.5 (b), and 0.75 (c).

CO molecules via the support is important in CO oxidation on model nanometer catalysts obtained by evaporating Pd onto mica (27), Al_2O_3 (28), SiO_2 (29) and MgO(100) (30). There are also a few theoretical treatments (Refs. (22, 23) and (31–34)) of this phenomenon.

The models, proposed by Aris *et al.* (31, 32), primarily focused on diffusion along the support toward catalytic islands, which were assumed to be widely separated (no interference of the diffusion zones) (31) or regularly distributed with overlapping diffusion zones (32) (see also Ref. (33, Chapter 7.5)). The reaction kinetics on the catalyst in those studies, however, have not been analyzed explicitly.

Henry (34) (see also Ref. (30)) has simulated CO oxidation on metal particles by combining CO diffusion on the support with the reaction steps on the catalyst. Diffusion jumps from the support to the metal were considered to be rapid and *irreversible* (mathematically, this means that the CO coverage on the support in the vicinity of the catalyst boundaries was assumed to be zero). This approximation is reasonable near the maximum of the reaction rate, but fails in the situation when the reaction rate is partly suppressed (poisoned) by CO adsorption.

Silveston *et al.* (22, 23) have analyzed the kinetics of a general reaction occurring via the LH mechanism on the surface containing two types of patches. One of them (metal) was assumed to have catalytic properties. The other one (support) was considered to act as a storage, communicating with the active phase via diffusion (spillover). On the support, adsorption/desorption processes were either allowed (Ref. (22)) or forbidden (Ref. (23)). Diffusion

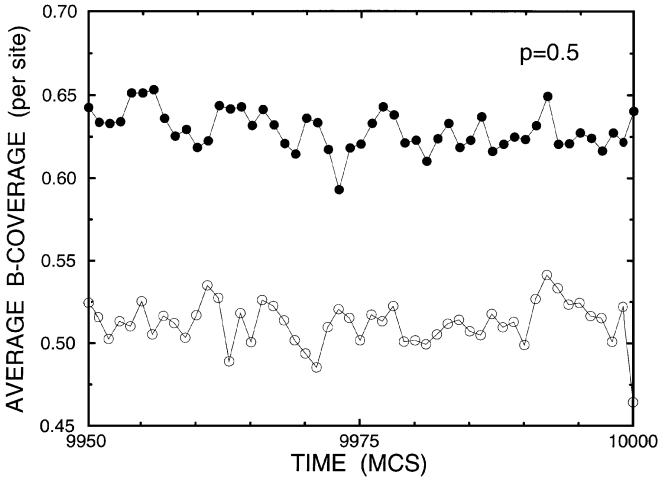

FIG. 7. Averaged (over sites) B coverage as a function of time (after every MCS) for a 50×50 lattice with periodic boundary conditions (filled circles) and with the boundary conditions described in the text (open circles). In both cases, the coverage fluctuations are not too high but certainly slightly higher than those predicted by the Poisson distribution (according to this distribution, the square root of the mean square fluctuation of the coverage, given by $(\theta_B)^{1/2}/L$ (26), should be about 0.015 for $\theta_B = 0.6$ and $L = 50$).

between patches was not treated explicitly. Instead, the authors (22, 23) employed ordinary differential equations (as in Refs. (10–12) discussed above) to describe the latter process. The main goal of both studies (22, 23) was to demonstrate that under periodically forced operation a catalytic system possessing a spillover-storage function might behave significantly differently from the same catalytic system without this property.

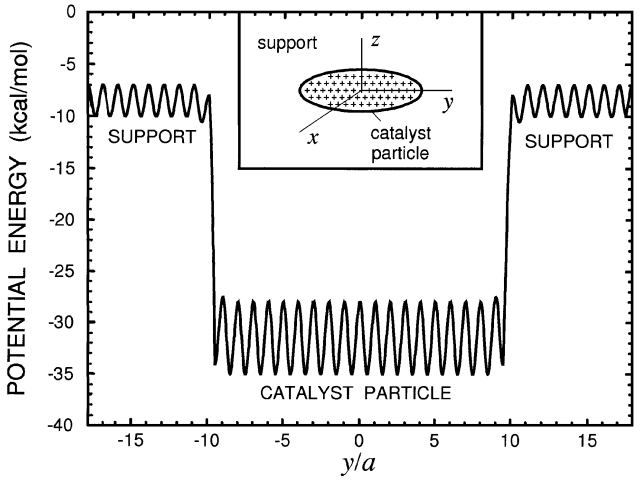

FIG. 8. Schematic potential energy, U (y), for A molecules on the surface (y is the coordinate along the surface). $U = 0$ corresponds to the gas phase. The binding energies for adsorption on the support and catalyst are 10 and 35 kcal/mol, and the activation energies for diffusion are, respectively, 3 and 7 kcal/mol. The inset shows a circular catalyst particle on the support.

General Equations

In our paper, we present the first *self-consistent* study of the kinetics of a catalytic reaction with significant reactant supply from the support; i.e., we explicitly treat diffusion of one of the reactants on the support and the reaction steps on the catalyst. As an example, we will again (as in Section 2) consider the $2A + B_2 \rightarrow 2AB$ reaction occurring via steps [1]–[3], but now A molecules are also allowed to adsorb on the support (B_2 adsorption on the support is neglected). The treatment will be done in the framework of the MF approximation (MC simulations of the reaction with reactant diffusion on the support are in principle possible but too cumbersome).

As already noted in Section 2, the kinetics of the reaction under consideration have been studied in detail for the infinite surface in the MF approximation and also in the case of limited mobility of the reactants. The conventional MF kinetic equations describing the reaction are

$$d\theta_A/dt = k_A^{\mathrm{a}} P_A (1 - \theta_A - \theta_B) - k_A^{\mathrm{d}} \theta_A - k_{\mathrm{r}} \theta_A \theta_B, \quad [13]$$

$$d\theta_B/dt = k_{B_2}^{\mathrm{a}} P_{B_2} (1 - \theta_A - \theta_B)^2 - k_{\mathrm{r}} \theta_A \theta_B, \quad [14]$$

where θ_A and θ_B are adsorbate coverages, P_A and P_{B_2} the reactant pressures, and k_A^{a}, k_A^{d}, $k_{B_2}^{\mathrm{a}}$, and k_{r} the rate constants for adsorption, desorption, and reaction.

To illustrate explicitly the type of kinetics predicted by Eqs. [13] and [14], we assume that the LH step is rapid, i.e., $k_{\mathrm{r}} \rightarrow \infty$. In this limit, the surface is (near the steady state) covered predominantly by A or B species. When P_A/P_{B_2} is small, the B_2 adsorption dominates (i.e., $\theta_B \gg \theta_A$ and $\theta \simeq \theta_B$, where $\theta = \theta_B + \theta_B$), the A coverage is low, and the A desorption rate is to a first approximation negligible due to rapid A reaction with B; i.e., the adsorption rate of A is balanced by the reaction, $k_A^{\mathrm{a}} P_A (1 - \theta) \simeq k_{\mathrm{r}} \theta_A \theta_B$. Substituting the latter relationship into Eq. [14], we have

$$d\theta/dt = k_{B_2}^{\mathrm{a}} P_{B_2} (1 - \theta)^2 - k_A^{\mathrm{a}} P_A (1 - \theta). \quad [15]$$

In analogy, the A dominated regime (where P_A/P_{B_2} is sufficiently large and $\theta \simeq \theta_A$) is described as

$$d\theta/dt = k_A^{\mathrm{a}} P_A (1 - \theta) - k_A^{\mathrm{d}} \theta - k_{B_2}^{\mathrm{a}} P_{B_2} (1 - \theta)^2. \quad [16]$$

Under the steady-state conditions, Eqs. [15] and [16] predict bistable kinetics (Fig. 9, dot-dashed curves). The spinodal point for the high-reactive regime occurs, according to Eq. [15], at $k_A^{\mathrm{a}} P_A = k_{B_2}^{\mathrm{a}} P_{B_2}$. For the low-reactive regime (Eq. [16]), the condition for the spinodal is easily obtained numerically.

To simulate a system of small, supported catalyst particles, the catalyst shape is here taken to be circular with radius R (Fig. 8). The reaction kinetics on the catalyst particles are assumed to be given by Eqs. [13] and [14] complemented by terms describing the flux of A particles from

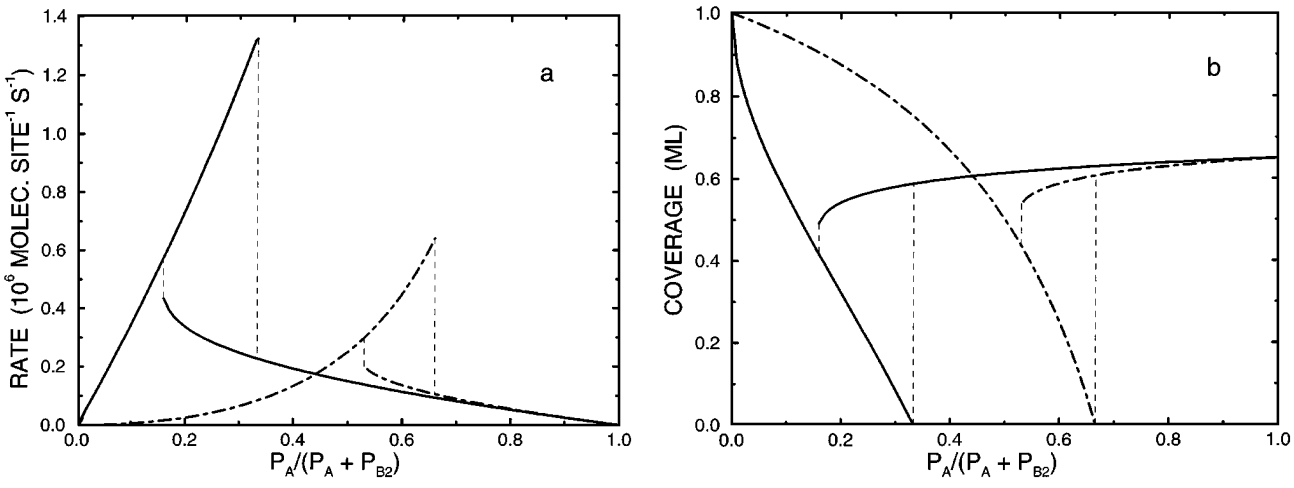

FIG. 9. (a) Reaction rate and (b) reactant coverages for rapid $2A + B_2 \rightarrow 2AB$ reaction under steady-state conditions. The dashed lines show the kinetics for the infinite adsorbed overlayer (Eqs. [13] and [14]). The solid lines correspond to reaction on the catalyst particles (Eqs. [24] and [31] with Eqs. [26] and [33] for P_A^{eff}, respectively). The input data for calculations are as follows: reaction conditions, $T = 450$ K, $P_A + P_{B_2} = 0.01$ bar; A adsorption, $k_A^{\text{a}} = 10^8\ \text{s}^{-1}\ \text{bar}^{-1}$; B_2 adsorption, $k_{B_2}^{\text{a}} = 2 \times 10^8\ \text{s}^{-1}\ \text{bar}^{-1}$; A desorption, $k_A^{\text{d}} = \nu_A^{\text{d}} \exp(-E_A^{\text{d}}/T)$; $\nu_A^{\text{d}} = 10^{16}\ \text{s}^{-1}$, $E_A^{\text{d}} = 35 - 15\theta_A$ kcal/mol; processes on the catalyst, $D\mathcal{K}_A^{\text{a}}/[R^2\mathcal{K}_A^{\text{d}}k_A^{\text{a}}\ln(l/R)] = 1.5$.

the support to the catalyst (this approach is reasonable if adsorbate diffusion on the active catalyst is rapid (i.e., no radial concentration gradients on the catalyst particles)). To calculate this flux, we need to solve the diffusion equation describing A particles on the support,

$$\frac{\partial \Theta}{\partial t} = \frac{D}{r}\frac{\partial}{\partial r}\left[r\frac{\partial \Theta}{\partial r}\right] + \mathcal{K}_A^{\text{a}} P_A - \mathcal{K}_A^{\text{d}}\Theta, \qquad [17]$$

where $\Theta \ll 1$ is the A coverage on the support ($\Theta \ll 1$ if the A binding energy on the support is sufficiently low, i.e., $\mathcal{K}_A^{\text{a}} P_A \ll \mathcal{K}_A^{\text{d}}$), D is the diffusion coefficient, and $\mathcal{K}_A^{\text{a}}$ and $\mathcal{K}_A^{\text{d}}$ are the rate constants for adsorption and desorption on the support, respectively.

The boundary condition for Eq. [17] at $r = R$ is given by

$$(D/a)\partial\Theta/\partial r\,|_{r=R} = k_{\text{eff}}\Theta(R), \qquad [18]$$

where a is the lattice spacing, $k_{\text{eff}}\Theta(R)$ the *net* flux (per boundary site) of A molecules from the support to the catalyst particle, and k_{eff} the "effective" rate constant connecting the net flux with $\Theta(R)$ (k_{eff} should be calculated by solving self-consistently Eqs. [17] and [15] or [17] and [16]).

Applying Eqs. [17] and [18], we will first treat the situation with widely separated catalyst particles (non-overlapping diffusion zones). Then, the solution obtained is generalized to the case of regularly distributed catalysts *with* overlapping diffusion zones.

Widely Separated Catalyst Particles

If the distance between catalyst particles is large, we can ignore the interference of the reaction kinetics on different particles and consider that $\Theta(r) = \mathcal{K}_A^{\text{a}} P_A/\mathcal{K}_A^{\text{d}}$ at $r \rightarrow \infty$. In this case, the steady-state solution to Eq. [17] is known to be

$$\Theta(r) = [1 - \mathcal{A}\,K_0(r/l)]\mathcal{K}_A^{\text{a}} P_A/\mathcal{K}_A^{\text{d}}, \qquad [19]$$

where $\mathcal{A} = 1/[K_0(R/l) - (D/alk_{\text{eff}})K_1(R/l)]$, $l = (D/\mathcal{K}_A^{\text{d}})^{1/2}$, $K_0(x)$ is a modified Bessel function of the second kind of zero order, and $K_1(x) = dK_0(x)/dx$ the corresponding function of first order.

For small catalyst particles, we may assume that $l \gg R$. In this limit, i.e., at $x = r/l \ll 1$, the asymptotic behavior of the Bessel function of zero oder is $K_0(x) \simeq -\ln(x)$, and and accordingly $K_1(x) \simeq -1/x$. Substituting these expressions into Eq. [19] results at $r = R$ in

$$\Theta(R) \simeq \left(D\mathcal{K}_A^{\text{a}} P_A/aR\mathcal{K}_A^{\text{d}}\right)/[k_{\text{eff}}\ln(l/R) + D/aR]. \qquad [20]$$

Inserting the latter expression into the right-hand part of Eq. [18], we obtain the net A diffusion flux per boundary site from the support to the catalyst particle. Multiplying this flux by the number of boundary sites ($\simeq 2\pi R/a$) yields the total diffusion flux to the catalyst particle,

$$F \simeq (2\pi R/a)k_{\text{eff}}\Theta(R) \simeq \frac{2\pi D\mathcal{K}_A^{\text{a}} k_{\text{eff}} P_A}{a^2\mathcal{K}_A^{\text{d}}[k_{\text{eff}}\ln(l/R) + D/aR]}. \qquad [21]$$

The flux per one site on the catalyst particle, $\mathcal{F}$, is obtained by dividing the total flux by the number of sites on the particle ($\approx \pi R^2/a^2$), i.e.,

$$\mathcal{F} \simeq \frac{2D\mathcal{K}_A^{\text{a}} k_{\text{eff}} P_A}{R^2\mathcal{K}_A^{\text{d}}[k_{\text{eff}}\ln(l/R) + D/aR]}. \qquad [22]$$

If the catalyst particle is primarily covered by B, the A molecules diffusing from the support to the catalyst are rapidly consumed due to reaction. In this case, A jumps onto the catalyst are irreversible, and $k_{\text{eff}} = (1-\theta)\mathcal{K}_{10}$, where $\mathcal{K}_{10}$ is the jump rate for the case when the spot is empty. Substituting this expression for k_{eff} into Eq. [22] yields

$$\mathcal{F} \simeq \frac{2D\mathcal{K}_A^{\text{a}}\mathcal{K}_{10}P_A(1-\theta)}{R^2\mathcal{K}_A^{\text{d}}[(1-\theta)\mathcal{K}_{10}\ln(l/R)+D/aR]}. \qquad [23]$$

Adding the flux [23] into Eq. [15], we get the following equation for the reaction on the catalyst particle in the B-dominated regime:

$$d\theta/dt = k_{B_2}^{\text{a}}P_{B_2}(1-\theta)^2 - k_A^{\text{a}}P_A^{\text{eff}}(1-\theta); \qquad [24]$$

here

$$P_A^{\text{eff}} \simeq \left(1+\frac{2D\mathcal{K}_A^{\text{a}}\mathcal{K}_{10}}{R^2\mathcal{K}_A^{\text{d}}k_A^{\text{a}}[(1-\theta)\mathcal{K}_{10}\ln(l/R)+D/aR]}\right)P_A \qquad [25]$$

is the effective A pressure (note that the form of Eq. [24] is similar to that of Eq. [15]).

If the A-consumption rate is high ($\mathcal{K}_{10} \gg D/aR$), the effective pressure is given by

$$P_A^{\text{eff}} \simeq \left(1+\frac{2D\mathcal{K}_A^{\text{a}}}{R^2\mathcal{K}_A^{\text{d}}k_A^{\text{a}}\ln(l/R)(1-\theta)}\right)P_A. \qquad [26]$$

The reaction rate is maximum when the impingement rates of A and B_2 are balanced and the catalyst particle is almost empty ($\theta \to 0$). In this case, Eq. [26] can be rewritten as

$$P_A^{\text{eff}} \simeq \left(1+\frac{2D\mathcal{K}_A^{\text{a}}}{R^2\mathcal{K}_A^{\text{d}}k_A^{\text{a}}\ln(l/R)}\right)P_A. \qquad [27]$$

The latter equation expresses that the "pressure" enhancement is proportional to the sticking coefficient and to the diffusion rate on the support and inversely proportional to the catalyst particle radius times the desorption rate constant on the support.

If the catalyst particle is primarily covered by A molecules, we must take into account A jumps both from the support to the catalyst and from the catalyst to the support. In this case, the *net* A flux (per boundary site) from the support to the spot is given by

$$k_{\text{eff}}\Theta(R) \equiv (1-\theta)\mathcal{K}_{10}\Theta(R) - \mathcal{K}_{01}\theta, \qquad [28]$$

where $\mathcal{K}_{01}$ is the rate constant for jumps from the catalyst onto the support. Solving Eq. [28] together with Eq. [19] (or with Eq. [20]), one can obtain explicit expressions for k_{eff} and $\Theta(R)$ and then for the flux $\mathcal{F}$. In particular, combining Eqs. [20] and [28], we have

$$\mathcal{F} \simeq \frac{2D\mathcal{K}_A^{\text{a}}\mathcal{K}_{10}P_A(1-\theta)\left[1-\mathcal{K}_{01}\mathcal{K}_A^{\text{d}}\theta/\mathcal{K}_{10}\mathcal{K}_A^{\text{a}}P_A(1-\theta)\right]}{R^2\mathcal{K}_A^{\text{d}}[(1-\theta)\mathcal{K}_{10}\ln(l/R)+D/aR]}. \qquad [29]$$

The rate constants in the expression above are interconnected via the relationships given by the detailed balance principle for the A adsorption–desorption equilibrium,

$$k_A^{\text{a}}P_A(1-\theta) = k_A^{\text{d}}\theta,$$
$$\mathcal{K}_A^{\text{a}}P_A = \mathcal{K}_A^{\text{d}}\Theta,$$
$$\mathcal{K}_{10}(1-\theta)\Theta = \mathcal{K}_{01}\theta.$$

These equations yield $\mathcal{K}_{01}\mathcal{K}_A^{\text{d}}k_A^{\text{a}} = \mathcal{K}_{10}\mathcal{K}_A^{\text{a}}k_A^{\text{d}}$. Substituting the latter relationship into the square brackets in the numerator of Eq. [29] results in

$$\mathcal{F} \simeq \frac{2D\mathcal{K}_A^{\text{a}}\mathcal{K}_{10}P_A(1-\theta)\left[1-k_A^{\text{d}}\theta/k_A^{\text{a}}P_A(1-\theta)\right]}{R^2\mathcal{K}_A^{\text{d}}[(1-\theta)\mathcal{K}_{10}\ln(l/R)+D/aR]}. \qquad [30]$$

Adding the flux [30] into Eq. [16], we obtain the kinetic equation for the A excess regime

$$d\theta/dt = k_A^{\text{a}}P_A^{\text{eff}}(1-\theta) - k_A^{\text{d}}\theta - k_{B_2}^{\text{a}}P_{B_2}(1-\theta)^2, \qquad [31]$$

where

$$P_A^{\text{eff}} \simeq \left(1+\frac{2D\mathcal{K}_A^{\text{a}}\mathcal{K}_{10}\left[1-k_A^{\text{d}}\theta/k_A^{\text{a}}P_A(1-\theta)\right]}{R^2\mathcal{K}_A^{\text{d}}k_A^{\text{a}}[(1-\theta)\mathcal{K}_{10}\ln(l/R)+D/aR]}\right)P_A. \qquad [32]$$

If the jumps from the support to the catalyst are rapid ($\mathcal{K}_{10} \gg D/aR$), the effective A pressure is given by

$$P_A^{\text{eff}} \simeq \left(1+\frac{2D\mathcal{K}_A^{\text{a}}\left[1-k_A^{\text{d}}\theta/k_A^{\text{a}}P_A(1-\theta)\right]}{R^2\mathcal{K}_A^{\text{d}}k_A^{\text{a}}\ln(l/R)(1-\theta)}\right)P_A. \qquad [33]$$

Eqs. [24] and [31] combined with the derived explicit expressions for P_A^{eff} form the basis for calculating the reaction kinetics in the situation when the diffusion length, $l = (D/\mathcal{K}_A^{\text{d}})^{1/2}$, is larger than the catalyst radius, R, but lower than the half-distance between catalyst particles, $\mathcal{L}$.

Catalysts with Overlapping Diffusion Zones

If the diffusion length is larger than the half-distance between catalyst particles, $l > \mathcal{L}$, we need to take into account the interference of the diffusion zones of different catalyst particles. Analyzing this case, we assume that the catalyst particles are regularly located on the surface (as, e.g., in Fig. 10). For this arrangement, one can in principle obtain a general analytical solution of the diffusion equation for A molecules. This solution is, however, cumbersome. We therefore focus on the most interesting limit and construct

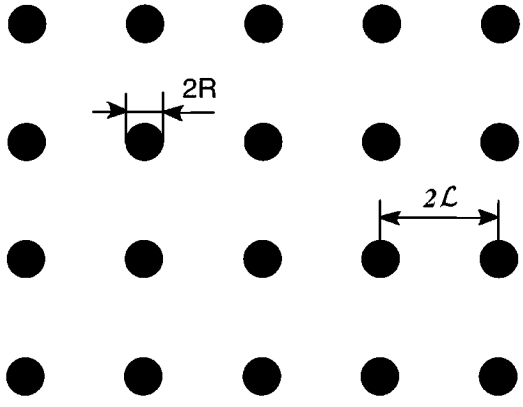

FIG. 10. Catalyst particles on the surface.

a solution corresponding to this limit. As in our former analysis, we are interested in the case when the catalyst size is small, $R \ll l$. Physically, it is clear that in this case the gradients in Θ (i.e., on the support) are established due to diffusion primarily at $r < l$. In this region, we may construct a fairly accurate solution to Eq. [17] by employing a few physically reasonable steps. First, we may at $r < l$ keep only the diffusion term in Eq. [17]. Elementary integration then yields

$$\Theta(r) = \mathcal{A} \ln(r) + \mathcal{B}, \qquad [34]$$

where $\mathcal{A}$ and $\mathcal{B}$ are arbitrary constants. Using the boundary condition [18], we obtain

$$D\mathcal{A}/aR = k_{\text{eff}}[\mathcal{A} \ln(R) + \mathcal{B}]. \qquad [35]$$

The second equation for $\mathcal{A}$ and $\mathcal{B}$ can be obtained by employing relevant boundary conditions at large r. In particular, for widely separated catalyst particles ($l < \mathcal{L}$), we may simply consider that Θ reaches the equilibrium value $\mathcal{K}_A^{\text{a}}/\mathcal{K}_A^{\text{d}}$ at $r = l$, i.e.,

$$\mathcal{A} \ln(l) + \mathcal{B} = \mathcal{K}_A^{\text{a}}/\mathcal{K}_A^{\text{d}}. \qquad [36]$$

Solving Eqs. [35] and [36], one can easily prove that at $r = R$, Eq. [34] is equivalent to Eq. [20], which was derived by using a general solution to Eq. [17]. This example illustrates that the method employed to construct a solution to Eq. [17] is rather accurate.

If $l > \mathcal{L}$, the second equation for $\mathcal{A}$ and $\mathcal{B}$ can be derived by taking into account that the *net* rate of A adsorption and desorption on the surface area around a given catalyst particle (at $r < \mathcal{L}$) should be equal to the A diffusion flux to this catalyst particle. The former value is defined as

$$W = \int_R^{\mathcal{L}} (2\pi r/a^2)\left[\mathcal{K}_A^{\text{a}} P_A - \mathcal{K}_A^{\text{d}} \Theta(r)\right] dr \simeq (\pi \mathcal{L}^2/a^2)\left[\mathcal{K}_A^{\text{a}} P_A - \mathcal{K}_A^{\text{d}}(\mathcal{A} \ln \mathcal{L} + \mathcal{B})\right].$$

The diffusion flux is given by $F = 2\pi D\mathcal{A}/a^2$. From the condition $W = F$, we have

$$\mathcal{L}^2\left[\mathcal{K}_A^{\text{a}} P_A - \mathcal{K}_A^{\text{d}}(\mathcal{A} \ln \mathcal{L} + \mathcal{B})\right] = 2\mathcal{A}D. \qquad [37]$$

Solving Eqs. [35] and [37], one can obtain explicit expressions for $\mathcal{A}$ and $\mathcal{B}$ and then find the A diffusion flux to the catalyst particle,

$$F \simeq \frac{2\pi D \mathcal{K}_A^{\text{a}} k_{\text{eff}} P_A}{a^2 \mathcal{K}_A^{\text{d}}\left[k_{\text{eff}} \ln(\mathcal{L}/R) + 2Dk_{\text{eff}}/\mathcal{K}_A^{\text{d}}\mathcal{L}^2 + D/aR\right]}. \qquad [38]$$

This equation plays the same role in the case of catalyst particles with overlapping diffusion zones as Eq. [21] for widely separated particles. Accordingly, the reaction kinetics taking into account the overlapping of diffusion zones can be obtained simply by repeating all the steps described after Eq. [21] (up to Eq. [33]).

Results of Calculations

To illustrate the effect of reactant supply via the support on the reaction kinetics, we will consider the case of widely separated catalyst particles. The analysis above indicates (see Eqs. [26], [27], and [33]) that the support-mediated channel is important if $D\mathcal{K}_A^{\text{a}}/R^2\mathcal{K}_A^{\text{d}}k_A^{\text{a}} > 1$. Often, $\mathcal{K}_A^{\text{a}} \simeq k_A^{\text{a}}$. Taking in addition into account that $D = a^2\Re$ ($\Re$ is the jump rate constant for diffusion), we can rewrite the condition above as $a^2\Re/R^2\mathcal{K}_A^{\text{d}} > 1$, or

$$\left(a^2\nu_{\text{dif}}/R^2\nu_{\text{des}}\right) \exp[(\mathcal{E}_{\text{des}} - \mathcal{E}_{\text{dif}})/T] > 1, \qquad [39]$$

where ν_{dif}, $\mathcal{E}_{\text{dif}}$, ν_{des}, and $\mathcal{E}_{\text{des}}$ are the Arrhenius parameters for A diffusion and desorption on the support, respectively. Usually, the activation energy for desorption is much higher than for diffusion. This is one of the two reasons why the support can act as an important source of reactant supply. The second reason is that for nanometer-size catalysts (with $R \sim 3$–10 nm) the ratio a^2/R^2 is not too low. On the other hand, the ratio of the pre-exponential factors $\nu_{\text{dif}}/\nu_{\text{des}}$ is often low (33). The latter may suppress the support channel (it can also be suppressed if the rate constant for jumps from the support to the catalyst, $\mathcal{K}_{10}$, is low, i.e., if there is a large activation barrier for these jumps). If for example $a^2/R^2 = 10^{-2}$, $\nu_{\text{dif}}/\nu_{\text{des}} = 10^{-2}$, and $T = 400$ K, the reactant supply via the support is important provided that $\mathcal{E}_{\text{des}} - \mathcal{E}_{\text{dif}} > 7$ kcal/mol. This requirement is realistic for CO adsorption on oxides (e.g., for MgO (35)).

Typical reaction kinetics calculated by employing Eqs. [24] and [31] (with Eqs. [26] and [33] for P_A^{eff}) are shown in Fig. 9 (solid lines). Due to the A supply from the support, the position of the maximum reaction rate is shifted to a lower value of the $P_A/(P_A + P_{B_2})$ ratio. In addition, the dependence of the reaction rate on the reactant pressure (for the regime where P_A is small and the surface is predominantly covered by B) is changed considerably (it becomes linear) compared to the case without A diffusion

from the support. As $P_A/(P_A + P_{B_2})$ increases from 0 to 1, the system exhibits a transition from a regime where the reaction rate is almost completely controlled by A supply from the support to a regime where diffusion from the support is negligible.

4. CONCLUSION

The results above clearly demonstrate that the kinetics on a faceted nanocrystal may be unique and distinctly different from that on a single crystal face, or on a superposition of different single crystal faces, because of the coupling of the kinetics on adjacent facets by surface diffusion. For the model case considered, the absolute rate at a given gas-phase composition, the position of the rate maximum vs mixing ratio, and the bistability regime are different from those for extended single crystal faces. Note that the former two results will hold even if the reaction rate is single valued (i.e., does not have a bistable regime). This theoretical result, together with a similar qualitative conclusion (7) based on the FIM study of the H_2–O_2 reaction on a Pt tip, has important implications for evaluation of practical catalyst systems: When measured catalytic conversion rates vs mixing ratio for supported catalysts are compared with the corresponding kinetics, one cannot *a priori* expect agreement with single crystal data (even if spillover effects are negligible), unless the active catalyst is totally dominated by one single crystal face or unless the reaction is structure insensitive. In the catalyst literature, differences between single crystal and supported catalyst kinetics are usually referred to as either spillover effect or so-called metal–support interaction (i.e., chemical modification of the catalyst particles by the support). There is no doubt that such an effect exist, but the present results signal a warning against drawing such conclusions so quickly. The alternative explanation that must be considered is that the observed kinetics is associated solely with the interplay of the reactions on different facets of nanocrystals.

With regard to the spillover kinetics presented above, the most important effects are that the rate maximum and the bistability regime appear at distinctly different compositions, compared to the case with no spillover. This intuitively expected result can be expressed in terms of an increased effective pressure of the reactant(s) supplied to the catalyst via adsorption on the support and diffusion to the catalyst. It was demonstrated that this can be a significant effect with *realistic* values of the rate constants and catalyst particle dimensions. Extensions of the spillover analysis should, e.g., include dissociative adsorption on the catalyst followed by diffusion to the support and reactions there.

For comparisons between the present type of analysis and experiments, the rapidly growing efforts to make model systems of supported catalysts by modern micro- and nanofabrication methods, are particularly interesting. Two-dimensional arrays of catalyst particles with monodisperse and well-defined sizes and interparticle distances can be manufactured and systematically varied in the ~10 nm range (2). The catalyst particles can be crystallized to monocrystal (2c), and so on. With such control, it will be possible to study experimentally in more detail the spillover effects, as well as the importance of the multifacet reaction kinetics.

APPENDIX: NOMENCLATURE

a	lattice spacing
A, B, B_2	reactants
D	diffusion coefficient
E, $\mathcal{E}$	activation energies
k^a, $\mathcal{K}^a$	rate constants for adsorption
k^d, $\mathcal{K}^d$	rate constants for desorption
k_{dif}	rate constant for diffusion
k_r	rate constant for reaction
$\mathcal{K}_{10}$, $\mathcal{K}_{01}$	rate constants for jumps near the catalyst/support boundary
k_B	Boltzmann constant
K_0, K_1	Bessel functions
l, l_{dif}	diffusion lengths
L	lattice size
$\mathcal{L}$	half-distance between catalyst particles
LH	Langmuir–Hinshelwood
MC	Monte Carlo
MCS	Monte Carlo step
p	dimensionless A impingement rate
p_1, p_2, p^*	critical parameters for kinetic phase transitions
P	pressure
r	coordinate of an adsorbed particle
R	radius of the catalyst particle
θ, Θ	adsorbate coverages
ν	pre-exponential factor

ACKNOWLEDGMENTS

We thank V. V. Gorodetskii for valuable discussions. Financial support for this work has been obtained from TFR.

REFERENCES

1. Kern, D., Ed., *J. Vac. Sci. Tech. B* **13**, 2321 (1995). [Proceedings of the International Conference on Electron, Ion, and Photon Beam Technology and Nanofabrication].
2. (a) Jacobs, P. W., Ribeiro, F. H., Somorjai, G. A., and Wind, S. J., *Catal. Lett.* **37**, 131 (1996); (b) Gunter, P. L. J., Niemantsverdriet, J. W., Ribeiro, F. H., and Somorjai, G., *Catal. Rev. Sci. Eng.* **39**, 77 (1997); (c) Wong, K., Johansson, S., and Kasemo, B., *Faraday Disc.* **105**, 30 (1996).
3. Shelef, M., and Graham, G. W., *Catal. Rev. Sci. Eng.* **36**, 433 (1994).
4. Zhdanov, V. P., and Kasemo, B., *Surf. Sci. Rep.* **20**, 111 (1994).
5. Imbihl, R., and Ertl, G., *Chem. Rev.* **95**, 697 (1995).

6. Zhdanov, V. P., and Kasemo, B., *Phys. Rev. B* **55**, 405 (1997).
7. Gorodetskii, V., Lauterbach, J., Rotermund, H.-H., Block, J. H., and Ertl, G., *Nature* **370**, 276 (1994).
8. Brosilow, B. J., Gulari, E., and Ziff, R. M., *J. Chem. Phys.* **98**, 674 (1993).
9. Savchenko, V. I., and Efremova, N. F., *React. Kin. Catal. Lett.* **57**, 49 (1996).
10. Savchenko, V. I., and Dadayan, K. A., *React. Kin. Catal. Lett.* **55**, 33 (1995).
11. Savchenko, V. I., *React. Kin. Catal. Lett.* **55**, 143 (1995).
12. Savchenko, V. I., Ivanov, E. A., and Fadeev, S. I., *React. Kin. Catal. Lett.* **57**, 55 (1996).
13. Gomer, R., *Rep. Progr. Phys.* **53**, 917 (1990).
14. Bär, M., Zülicke, Ch., Eiswirth, M., and Ertl, G., *J. Chem. Phys.* **96**, 8595 (1992).
15. Wintterlin, J., Schuster, R., and Ertl, G., *Phys. Rev. Lett.* **77**, 123 (1996).
16. Xu, M., Liu, J., and Zaera, F., *J. Chem. Phys.* **104**, 8825 (1996).
17. Hellsing, B., Kasemo, B., and Zhdanov, V. P., *J. Catal.* **132**, 210 (1991).
18. Verheij, L. K., Freitag, M., Hugenschmidt, M. B., Kempf, I., Poelsema, B., and Comsa, G., *Surf. Sci.* **272**, 276 (1992).
19. Ziff, R. M., Gulari, E., and Barshad, Y., *Phys. Rev. Lett.* **56**, 2553 (1986).
20. Lutsevich, L. V., Elokhin, V. I., Myshlyavtsev, A. V., Usov, A. G., and Yablonskii, G. S., *J. Catal.* **132**, 302 (1991).
21. Conner, W. C., and Falconer, J. L., *Chem. Rev.* **95**, 759 (1995).
22. Edvinsson, R. K., Hudgins, R. R., and Silveston, P. L., *in* "New Aspects of Spillover Effects in Catalysis" (T. Inui *et al.*, Eds.), p. 229. Elsevier, Amsterdam, 1993.
23. Nam, Y. W., and Silveston, P. L., *in* "New Aspects of Spillover Effects in Catalysis" (T. Inui *et al.*, Eds.), p. 235. Elsevier, Amsterdam, 1993.
24. Silverberg, M., and Ben-Shaul, A., *J. Chem. Phys.* **87**, 3178 (1989).
25. Tammaro, M., Sabella, M., and Evans, J. W., *J. Chem. Phys.* **103**, 10277 (1995).
26. Landau, L. D., and Lifshitz, E. M., "Statistical Physics," Pergamon Press, Oxford, 1993.
27. Matolin, V., and Gillet, E., *Surf. Sci.* **166**, L115 (1986).
28. Rumpf, F., Poppa, H., and Boudart, M., *Langmuir* **4**, 722 (1988).
29. Eriksson, M., and Petersson, L.-G., *Surf. Sci.* **311**, 139 (1994).
30. Becker, C., and Henry, C. R., *Surf. Sci.* **352**, 457 (1996).
31. Aris, R., *J. Catal.* **22**, 282 (1971).
32. Kuan, D.-J., Davis, H. T., and Aris, R., *Chem. Eng. Sci.* **38**, 719 (1983).
33. Zhdanov, V. P., "Elementary Physicochemical Processes on Solid Surfaces," Plenum, New York, 1991.
34. Henry, C. R., *Surf. Sci.* **223**, 519 (1989).
35. He, J.-W., Corneille, J. S., Estrada, C. A., Wu, M.-C., and Goodman, D. W., *J. Vac. Sci. Techn. A* **10**, 2248 (1992).